Journal of Alloys and Compounds xxx (xxxx) 176390

Contents lists available at ScienceDirect

Journal of Alloys and Compounds

journal homepage: www.elsevier.com/locate/jallcom

Preparation, structural, electrical, and ferroelectric properties of solid and lead zirconium titanate ink

Mohamed Mustafa Dabour [a], Mahmoud Ahmed Mousa [a], Khaled Faisal Qasim [b]

[a] Chemistry Department, Faculty of Science, Benha University, Benha 13511, Egypt
[b] Chemistry Department, Faculty of Science, Suez University, Suez 43221, Egypt

ARTICLE INFO

Keywords:
Lead zirconium titanate
Piezoelectric ink
Ceramic
Electronic ink

ABSTRACT

The novelty of the work lies in the design and development of a significantly low-cost lead zirconate titanate (PZT) ink similar in its electrical properties to its original solid materials, which can be used for 3-D printing to print electronic circuits, shape memory, and devices quickly. The Zr/Ti = 52/48 ratio was achieved during the solid-state reaction to create the PZT powder. XRD, FT-IR, and SEM characterized the synthesized material. The PZT powder was found to form in a tetragonal phase. The PZT powder was used to prepare PZT ink with a 13 % Wt/Wt solid content composition. The ink's rheological characteristics and physical properties, such as particle size distribution, surface tension, viscosity, and electrical properties, were studied. Dielectric properties like dielectric constant (ε') and dielectric loss (ε'') indicate the poly-dispersive nature of the material. The temperature-dependent dielectric constant (ε') curve indicates relaxor behavior with a maximum at high temperatures. The poly-dispersive nature of the material was analyzed using Cole-Cole plots. The frequency dependence of AC conductivity follows the universal power law. The temperature dependence of dc-conductivity follows the Arrhenius law, with an activation energy of 0.14 eV at lower temperatures and 0.85 eV at higher temperatures. The electrical conductance study showed that PZT ceramic can be used in electronic circuits because of its high resistivity value and small temperature coefficient of resistance. The piezoelectric measurement displays d33 as 129 pC/N at room temperature.

1. Introduction

Modern technologies have increased the need for electronics, which has increased electrical garbage [1,2]. Over the past few decades, a revolutionary technology known as printed electronics (P.E.) has emerged, offering a solution to minimize electronic waste while enabling large-scale production at a low cost [3,4]. This innovative technology creates a wide range of devices, such as photovoltaic cells, solar panels, energy harvesters, batteries, light sources, and sensors, all on incredibly thin, lightweight, and flexible substrates [5]. The most crucial aspect of the electronic printing process is the physical characteristics of electronic ink (E-ink) [3]. Dielectric ink is a type of E-ink in addition to conductive and semi-conductive ink [6]. Lead zirconate titanate (PZT) is a high-temperature, low-loss ferroelectric ceramic material with a wide range of applications, including capacitors, piezoelectric transducers, sensors, and actuators. Therefore, the ZPT ceramic is a suitable choice for use as a functional ingredient in dielectric and piezoelectric ink [7].

PZT ceramic materials are a binary solid solution of ferroelectric $PbTiO_3$ and antiferroelectric $PbZrO_3$ with different Zr/Ti ratios. They belong to the perovskite family of a general formula ABO_3, with site A occupied by Pb^{2+} ions and site B by Zr^{4+} and/or Ti^{4+} ions [8]. PZT ceramics are susceptible near the morphotropic phase boundary (MPB) due to spontaneous polarization in different directions over a wide range of temperatures. They can be used in various applications such as charge storage, ferroelectric memories, MEMS, FRAM, transducer, oscillators, pyroelectric devices, actuators, and sensors [9–14].

Currently, the ferroelectric community has also been focusing on lead-free ferroelectric and antiferroelectric materials. Enhanced energy densities have been attained in ferroelectric ceramics (1-x)$BaTiO_{3\text{-}x}Bi(Mg_{1/2}Zr_{1/2})O_3$ (1.3 J/cm^3) [15], $(Na_{0.5}Bi_{0.5})TiO_3$-based (2.7 J/cm^3) [16], $(Na_{0.25}Bi_{0.25}Sr_{0.5})(Ti_{0.8}Sn_{0.2})O_3$ (3.4 J/cm^3) [17], $AgNbO_3$ (4.2 J/cm^3) [18,19], and $NaNbO_3$ (12.2 J/cm^3) [20].

However, the main reason for using PZT materials is that they can be synthesized on a large scale through a standard solid-state route of mixing, which is cost-effective [17]. Further, the existing physical properties of PZT can be altered through different preparation techniques, such as doping, grain size reduction, compositing, heating, etc. [21,22]. Moreover, the PZT with a 52:48 Zr/Ti ratio near MPB changes the intrinsic properties of PZT ceramics for a wide range of temperatures, as the MPB line is nearly vertical in the phase diagram. Hence, PZT has become a widely used and investigated material for the above mentioned applications [23,24].

Different methods can synthesize the ferroelectric materials to produce different morphologies [24–27]. However, in the present work,

https://doi.org/10.1016/j.jallcom.2024.176390
Received 5 April 2024; Received in revised form 9 June 2024; Accepted 5 September 2024
0925-8388/© 20XX

the PZT ceramics powder with the Zr/Ti ratio composition of 52:48 near MPB has been synthesized by solid-state reaction, and 13 % wt/wt aqueous ferroelectric ink has been prepared. The rheological characteristics and physical properties, including particle size distribution, surface tension, viscosity, and dry ink's electrical properties, were studied to investigate its ability to fabricate electronic circuits in inkjet.

The study presents the synthesis of $Zr_{0.52}Ti_{0.48}O_3$ ferroelectric powder by solid-state reaction. 13 % wt/wt ferroelectric inkjet can be used in electronic circuits. It also studies the rheological characteristics and physical properties, including particle size distribution, surface tension, viscosity, and electrical properties.

2. Experimental

Lead tetroxide (Pb_3O_4) 98 % was purchased from Merk, titanium dioxide (TiO_2) 98 % was provided from Alpha Chemical India, zirconium oxide (ZrO_2) 99 % was supplied from BDH England, polyvinylidene fluoride (PVDF) was purchased from Fluka France (M.wt = 534,000 g/mole), Polymethylmethacrylate (PMMA) was purchased from Sigma Aldrich (M.wt = 13,000 g/mole).

2.1. Preparation of nano PZT

The solid-state reaction technique [28] was modified in the following ways to produce lead zirconium titanate: First, 5.975 gm of Pb_3O_4, 0.983 gm of TiO_2, and 1.632 gm of ZrO_2 (Zr/Ti = 52/48) were mechanically activated for 72 hours in a planetary ball mill (Model Fritsch Pulverisatte-5). As milling media, a stainless steel vial (500 cm^3 vol.) was filled with powders and 20 mm stainless steel balls. The ball-to-powder weight ratio (BPR) of 100:1 was used. Next, the mixture was gradually pressed into a pellet shape at 120 MPa, and lastly, it was heated for seven hours at 900 °C. The pellets were heated in a covered alumina crucible to prevent metal oxide from evaporating and losing during heating. Moreover, the product analyzed by X-ray fluorescence showed the same elemental composition as the starting materials with an error value of 0.5 %.

2.2. Preparation of nano PZT ink

In a ball mill, 6.79 gm PZT, 0.29 gm PMMA as a binder, and a small amount of deionized water were combined for four hours. After that, 0.2 g PVDF was added as a dispersion agent. Finally, the solution was brought up to 50 milliliters and shaken at 300 rpm for 4 hours.

2.3. Characterizations

The particle size distribution of PZT ink was analyzed using the laser diffraction particle size analyzer Malvern Mastersizer 3000. The rheological properties of the ink were tested using a rotational rheometer. The crystal structure of the as-prepared PZT powder was characterized by XRD (Rigaku, model D/Max-2500/P.C.) using CuKα radiation in the 2θ range from 20^{O} to 80^{O} with a scanning rate of 0.02/min. Then, the X-ray results for the sample are compared using the match program to ensure that the required compound has been obtained. The morphology and microstructure of the as-prepared PZT were observed by a scanning electron microscope (JEOL JSM 6460 LV). FT-IR spectrum was recorded using SHIMADZU–IR in the frequency range of 400–4000 cm^{-1} with a resolution of 1 cm^{-1}. Dielectric studies were conducted on PZT of dry ink (under vacuum at 200 ^{O}C) in the form of a pressed pellet with a diameter of 7 mm and a thickness of 1 mm. The Hioki 3532–50 LCR Hi-Tester and a traditional two-terminal sample holder were used. To make the sample function like a parallel capacitor, air-drying silver paste was applied to both sides of the sample. The studies were conducted at frequencies ranging from 50 Hz to 5 MHz, from 313 K to 773 K. Ohmic contacts were created using gold electrodes. DC bulk resistivity was measured by using a guard ring method. Before the piezoelectric test, the sample was polled in silicon oil at 50 kV/cm for 30 min at 100°C, and the electric field was maintained during cooling at 50°C. The d33 value was measured by a d33 meter (PiezoMeter PM300, Piezotest).

3. Results and discussion

3.1. Nano PZT characterization

Fig. 1.a shows the XRD patterns of the as-prepared PZT sample. The XRD patterns illustrated the formation of PZT tetragonal phase structure as a significant product according to JCPDS card No. 50–0346 with diffraction peaks at 21.8°, 31.04°, 38.4°, 44.3°, 45.07°, 49.9°, 55.02°, 64.7 and 69.4° referring to (001), (101), (111), (200), (002), (102), (112), (202) and (212) plans, respectively. The sample's crystallite size (D_{XRD}) was estimated from diffractogram data at the highest peak intensity (110) using the Debye Scherrer formula [29]

$$D_{XRD}\frac{k\lambda}{\beta\cos\theta} \tag{1}$$

The D_{XRD} value is 14.5 nm, which is in the nanometer range. Because PZT exhibits a tetragonal crystal structure, the lattice parameters (a, c) are evaluated by using the following Equation [30]

$$\frac{1}{d_{hkl}^2} = \frac{h^2+k^2}{a^2}+\frac{l^2}{c^2} \tag{2}$$

Where (hkl) are the Miller indices, (d_{hkl}) is lattice space. The calculated lattice parameters are a = 4.02 ± 0.0041 Å and c = 4.085 ± 0.0044 Å, which agree well with those reported in the literature[31].

FT-IR results presented in Fig. 1.b confirm the formation of the perovskite structure of PZT-NPs. The Figure shows a broadband at about 750–400 cm^{-1} related to Ti(Zr)–O vibrations (ZrO_6, Ti-O_6, Zr–O and Ti-O for $Pb(ZrTi)O_3$ structures) [32,33].

The SEM image of the PZT sample is shown in Fig. 1.c. The micrographs show dense PZT ceramics with grain sizes of particles of approximately 50– 400 nm. The EDX analysis Fig. 1.d confirms the presence of titanium (13.88 %), oxygen (39.51 %), lead (30.57 %), and zirconium (16.04 %). These results provide validation that the PZT compound formed without detecting any unexpected impurities. Also, X-ray fluorescence results of PZT particles demonstrated that the atomic ratio of Zr: Ti = 24.15:22.41 = 1.0776, which is close to that in $Pb(Zr_{0.52}Ti_{0.48})O_3$ about 1.083 [8].

3.2. PZT ink characterization

The particle size distribution of PZT ink was analyzed employing the laser diffraction particle size analyzer (Malvern Mastersizer 3000), and the results are shown in Fig. 1.e. Most particles are small, and the values of D_{10}, D_{50}, and D_{90} are 0.0184, 0.0480, and 0.146 µm, respectively. The particle size distribution of a powder, D_{50}, is often used as the average particle size, so the average particle size is 0.0480 µm for PZT in ink with a surface area of 20.02 m^2/g; the higher surface area confirms the small particle size of PZT.

The ink's rheological characteristics fall within the limits of inkjet and aerosol printing devices [4]. At 30 °C, the surface tension is 35.5 mN/m, and the ink viscosity is 1.3 cp.

3.3. Impedance studies

Fig. 2.a shows the complex impedance spectrum of PZT ceramics (Z′ Vs. Z", Nyquist plot) as a function of frequency recorded at different temperatures. The appearance of a temperature-dependent semicircular arc characterizes this spectrum. The absence of low-

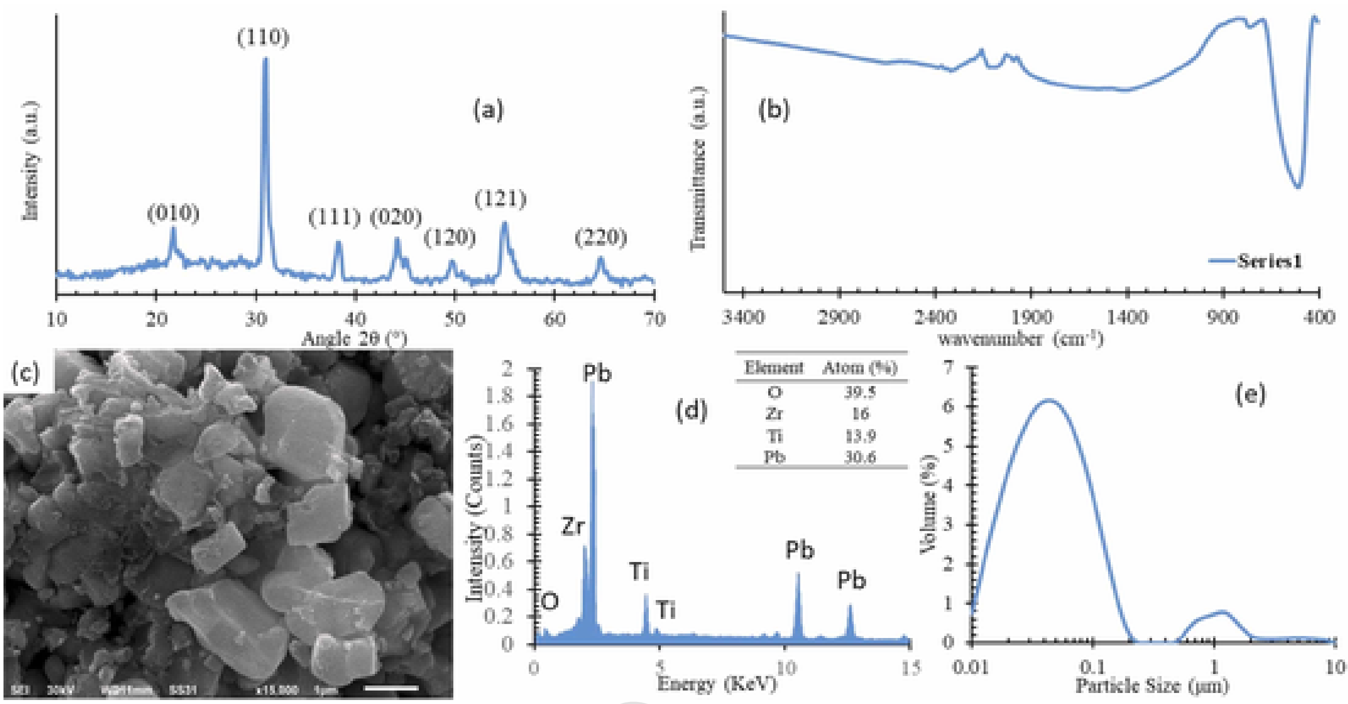

Fig. 1. a) XRD, b) FT-IR, c) SEM, d) EDX, e) particle size distribution of PZT.

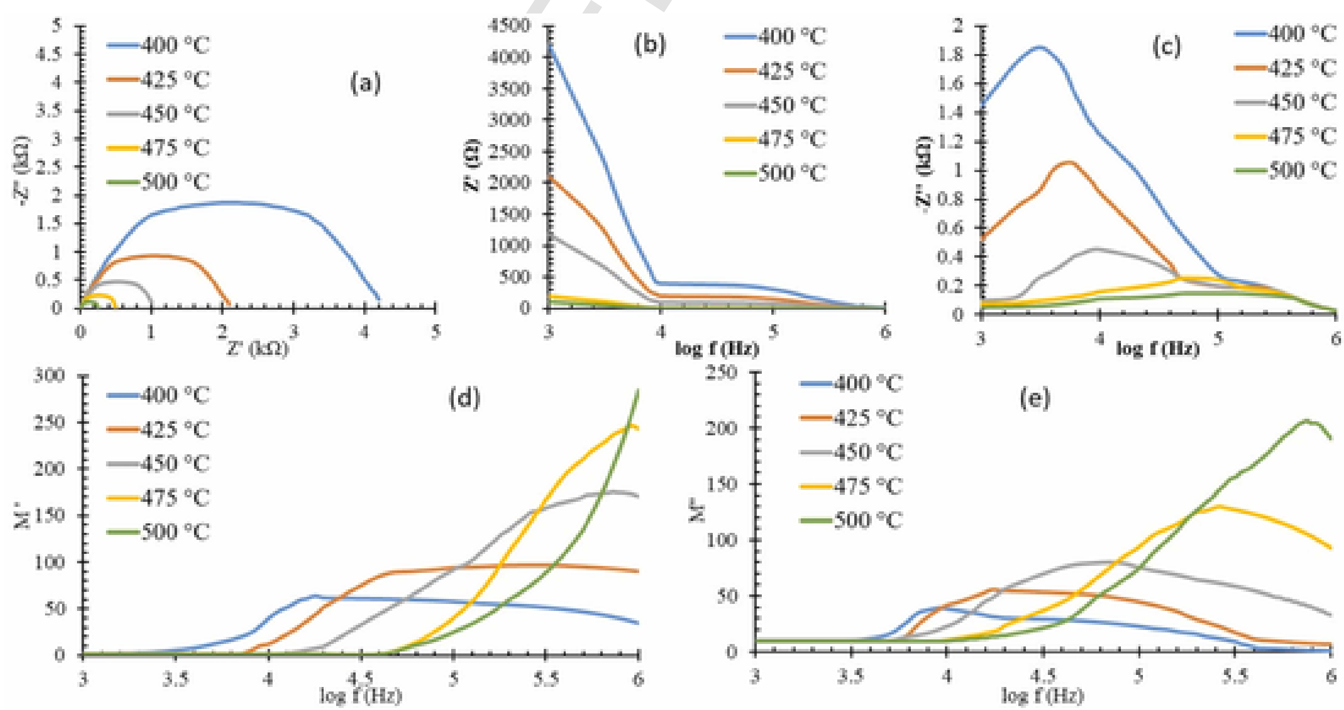

Fig. 2. a) Nyquist plot, Effect of frequency on b), c) impedance, d), e) modulus of PZT.

frequency semicircle indicates the presence of poorly resolved grain boundary components. Therefore, the material conduction/electrical response process is mainly due to its bulk property. Plots of this kind imply that (i) depressed semicircles signify the existence of non-Debye-type relaxation, and (ii) single semicircles are a result of the bulk property of the materials [34]. The point of intersection (i.e., intercept) of the semicircle on the Z-axis (i.e., x-axis) decides the sample's bulk resistance value. The Nyquist plot shows that as the temperature rises, the interception points have moved in the direction of the origin, indicating a decrease in the resistive property and an increase in the dc-conductivity of the material [35]. The tendency of R_b values to decrease with rising temperature indicates the presence of the negative temperature coefficient of resistance (NTCR) in materials like insulators and semiconductors [36]. Based on the above data, the material's electrical circuit will parallelly combine bulk capacitance and resistance.

Fig. 2.b shows the real component of impedance ($Z^{/}$) variation as a function of frequency at some selected high temperatures. $Z^{/}$ decreases with increasing frequency at all temperatures, signifying increased ac conductivity with frequency [37]. At lower frequencies, the reduction in the magnitude of $Z^{/}$ with the increase in the temperature reveals its NTCR behavior resembling the semiconductor or insulator behavior of materials [38–40]. $Z^{/}$-plots exhibit a total merging beyond a particular frequency, and their behavior alters significantly at high frequencies. This is attributed to the release of space charge and the ensuing reduction of the material's barrier properties [41].

Fig. 2.c shows the imaginary impedance component ($Z^{//}$) at different temperatures as a function of frequency (loss spectrum). The plot offers information about the electrical processes with the largest resistances and is appropriate for determining the most resistant component's relaxation frequency. The low-frequency dispersion and the merging at higher frequencies in this loss spectrum are caused by space charge polarization, which is present at lower frequencies and eliminated at higher frequencies. The peak's emergence at high temperatures signifies the material's electrical relaxation. The relaxation process may be explained by the existence of immobile or mobile species (electron species) at low temperatures and by vacancies and/or defects at higher temperatures [38–42]. The peak pattern widening asymmetry signifies a departure from the optimal Debye behavior. For a given set of materials, the relaxation frequency (f_{max}) is the frequency at which the value of $Z^{//}$ reaches a maximum, $Z^{//}{}_{max}$. With rising temperatures, f_{max} moves into a higher frequency area [43]. The peaks' widening and $Z^{//}$ max's decreasing value as temperature rises indicate the possibility of the temperature-dependent relaxation phenomena [44]. In high-temperature observations, the relaxation species-like defects might be the reason behind the Process of electrical conduction in the material [45,46]. The hopping of conduction electrons/oxygen ion vacancies/defects between the available localized sites is responsible for the electrical conduction/electrical transport process [38].

3.4. Modulus studies

Complex electric modulus is a widely recognized tool for analyzing materials' electrical response, including the nature of polycrystalline in samples and the electrical relaxation in electronically and ionically conducting materials [47].

The dielectric treatments and conductivity relaxation are less effective than the electric modulus in examining relaxation phenomena. This is because ε′, tan δ is suppressed at low frequencies, resulting in a large value. The complex electric modulus ($M^* = 1/\varepsilon^*(\omega) = M^{/} + jM^{//} = j\omega\, C_o\, Z^*$), where $M^{/}$ and $M^{//}$ are often referred to as the real and imaginary components of the modulus, can be used to analyze the electrical response of the materials. This formalism communicates the relaxation of the electric field in the material by saving electric displacement constant and provides vision into the bulk response using its capacitive nature [48].

The real ($M^{/}$) and imaginary ($M^{//}$) segments of electrical modulus at room temperature were calculated using Eq. (3) and Eq. (4) [49], respectively, and the outcomes are represented in Fig. 2.d,e.

$$M^{/} = \omega\, C_o\, Z^{//} \tag{3}$$
$$M^{//} = \omega\, C_o\, Z^{/} \tag{4}$$

C_o is the vacuum capacitance and is determined by

$$C_o = \frac{\varepsilon o.A}{t} \tag{5}$$

ε_o is the permittivity of free space) 8.854 $\times 10^{-12}$ F/m(, t is the thickness (m), and A is the area (m^2).

Fig. 2d shows how $M^{/}$ varies with the frequency sample across a large temperature range (400–500 ^{O}C). The modulus spectrum ($M^{/}$) varies across the temperature, with zero in the lower frequency range, continuous dispersion in the mid-frequency band, and a maximum in the higher frequency zone. The peak in $M^{/}$ at low-frequency regions at lower temperatures indicates charge carrier mobility over long distances, while the peak towards high-frequency regions indicates charge carriers' spatial confinement and mobility over short distances [50]**.** The peak value represents the material's dielectric spin relaxation process, with a broader peak on either side due to the non-Debye nature of the material, indicating a transition from long to short-range mobility with an increase in frequency [51].

Fig. 2.e demonstrates the variation of the imaginary part of the modulus ($M^{//}$) concerning frequency at selected temperatures. The investigated frequency range displays an asymmetrical peak (or its propensity) in both the low- and high-frequency regions. This observation indicated the absence of electrode polarization in the material. The temperature dependence of asymmetric broadening of the peak is monitored, which approves the broadening of relaxation with varying time constants [52]. Thus, the relaxation in the material is regarded as non-Debye type [53]. The plot also demonstrates how the peak shifts toward the higher frequency side as the temperature rises. This is consistent with the theory that the material's dielectric relaxation is caused by a thermally activated process in which intrinsic hopping of charge carriers with small polarons dominates. The low-frequency peak indicates the upper limit of frequencies at which charge carriers can hop to travel farther between sites, while the other peak shows the shift from short-range to long-range mobility on a decreasing frequency [54]. Only limited movements can be performed by the ions in the high-frequency range because they are spatially restricted to their potential wells [46].

The modulus $M^{//}$ and impedance $Z^{//}$ differentiate microscopic processes for localized dielectric relaxation and long-range conduction. Combining these plots with frequency helps determine the dominant movement of charge carriers. If the plots overlap, long-range movement is indicated, while separation reveals short-range transport dominates the relaxation process [55]. Fig. 2.c,e show a significant mismatch in the temperatures between $Z^{//}$ and $M^{//}$ peaks, indicating localized charge carriers and no contribution to long-range conduction [56].

3.5. Dielectric studies

The dielectric analysis is a crucial feature that can extract information about a material medium's electrical characteristics as a function of frequency and temperature [57]. The results of this analysis allow for the evaluation of the material's capacity to store and transfer electric charge. Eq. (6) is used to get the PZT sample's dielectric constant ($\varepsilon^{/}$)

$$\varepsilon^{/} = \frac{Ct}{\varepsilon_o A} \tag{6}$$

where C is capacitance (F), ε_o is the permittivity of free space) 8.854 $\times 10^{-12}$ F/m(, t is the thickness (m), and A is the area (m^2).

Fig. 3.a shows the variation of $\varepsilon^{/}$ at different frequencies with temperature increments for the tested sample. The dielectric constant increases gradually with temperature, with a modest rise from 30 to 180 ^{O}C due to weak charge carrier feedback. Beyond 180 ^{O}C, a steep rise is observed. $\varepsilon^{/}$ variation is a broadened curve, characteristic of a disorder perovskite structure with a diffuse phase transition, due to the complex occupation of the A and B sites by Pb^{2+}, Zr^{4+}, and Ti^{4+} ions [58]. Compositional fluctuation and/or substitutional disordering in cation arrangement leads to microscopic or nanoscopic heterogeneity in a compound, with different local Currie points [59]. Changes are attributed to lead vacancies and increased domain wall mobility. The dielectric constant decreases with frequency, indicating typical behavior of ferroelectric and/or dielectric materials [60]. Polarization does not oc-

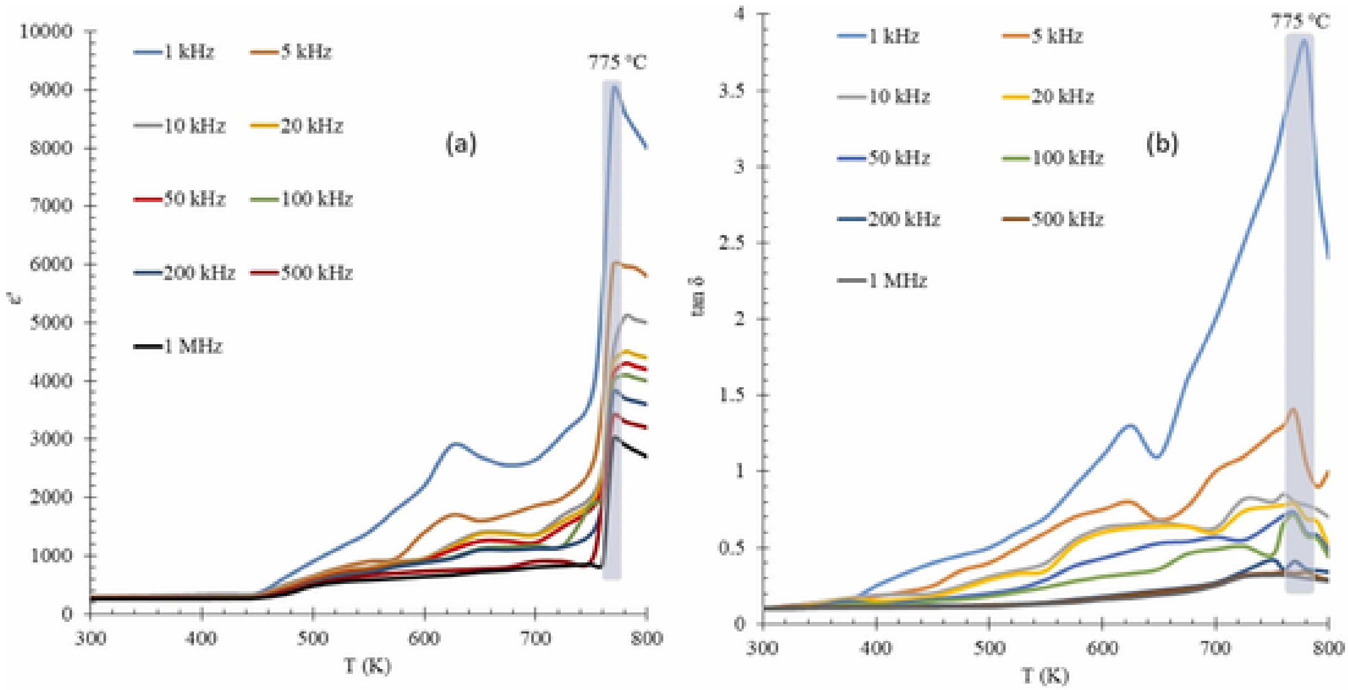

Fig. 3. Effect of frequency on a) dielectric constant, b) tangent loss.

cur instantaneously with the electric field due to charges' inertia. Higher values of ε' at lower frequencies are due to simultaneous presence of all types of polarization, which decreases with frequency [61]. At high frequencies, only electronic polarization exists in the materials [62].

Fig. 3.b shows the variation of dielectric loss tangent with temperature and frequencies for the tested sample. The dielectric loss factor behaves similarly to ε', increasing as temperature rises, facilitating dipole orientation and reaching maximum value before phase change [63]. The rapid increase in the dielectric losses at higher temperatures is attributed to the increase in dipole orientation and the presence of higher electric conduction in the paraelectric phase of the sample [64].

3.6. Conductivity studies

The dc-electrical conductivity was more than 10^{10} ohm/cm at room temperature, referring to insulating behavior. The temperature dependence of dc-conductivity at a temperature range between 50 and 500 ^{o}C is represented in Fig. 4.a. The Figure shows an Arrhenius behavior with an activation energy of 0.14 eV at temperatures lower than 135 ^{o}C, 0.99 eV at temperatures between 135 and 400 ^{o}C and 0.85 eV at temperatures > 400 ^{o}C. The higher drift mobility of thermally activated charge carriers is linked to the temperature-dependent rise in σ_{dc} values [65]. The primary causes of the dc- conductivity in ferroelectrics include defect dipolar effects, cation vacancies, and oxygen vacancies [66]. The ionization process, driven by electrons and holes, is the main component at low temperatures. In turn, electrical conductivity at higher temperatures is caused by the mobility of extrinsic defects, which may be connected to the oxygen lost during the sintering Process at high temperatures. The study indicates that the PZT ceramic, which has been prepared, is suitable for electronic circuits due to its high resistivity value and small temperature coefficient of resistance [67].

The frequency dependence of AC conductivity was examined to learn more about the electrical characteristics of the materials [68]. Fig. 4.b shows the PZT sample's frequency- and temperature-dependent conductivity. The formula below was used to compute the ac-conductivity [60].

$$\sigma_{ac}(\omega) = \omega\, \varepsilon_o\, \varepsilon^{//} \tan\delta \quad (7)$$

Plotting ln σ_{ac} of the PZT sample at various frequencies against the inverse absolute temperature (10^3/T) is depicted in Fig. 4.c. The curve's extensive temperature fluctuation pattern at higher temperatures validates the materials' temperature-dependent transport characteristics according to the Arrhenius equation[69]:

$$\sigma = \sigma_o \exp(-E_a / K_B T) \quad (8)$$

Where σ_o, E_a, and K_B are pre-exponential factors, activation energy, and Boltzmann constant, respectively. A rise in conductivity around CT indicates that the material is becoming more polarizable. According to the slope of Arrhenius plots, the estimated values of E_a are 0.34 eV at 200 kHz in the ferroelectric (FE) phase (230–440 ^{o}C) and 0.36 eV in the paraelectric (PE) phase > 440 ^{o}C).

The ac conductivity behavior can be explained by Jonscher's power law equation, i.e., universal power law [70]

$$\sigma_{ac} = \sigma_{dc} + A\omega^{n}\ (0 < n < 1) \quad (9)$$

Where n is the degree of interaction between the mobile ions and lattices, and A is a thermally activated, constantly defining polarisability intensity [71]. Both n and A are thermally activated quantities. AC conductivity spectra at different temperatures are fitted (the continuous line is shown in Fig. 4.b) with the power-law equation and extracted the several parameters σ_{dc}, A, and n, shown in Table 1. The table shows that the exponent n values consistently fall below 1 at different temperatures and decrease with temperature increase, based on charge carrier hopping over potential barriers, which aligns with experimental findings.

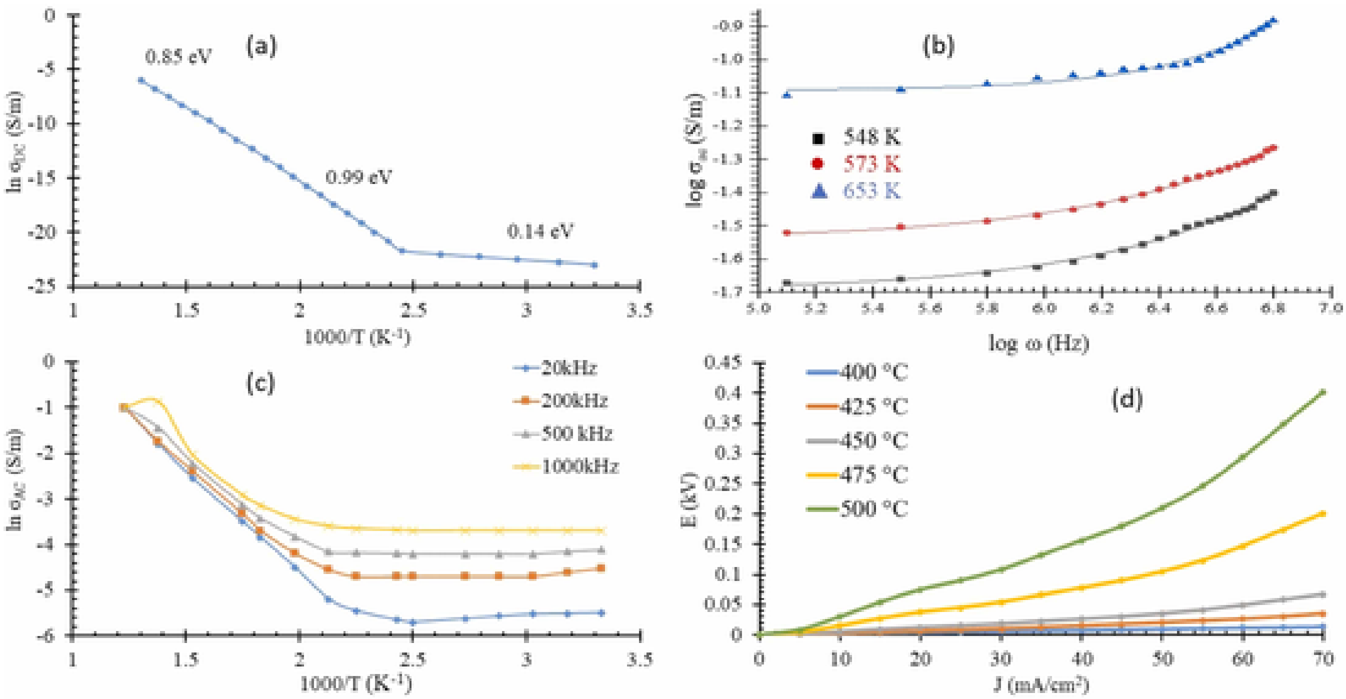

Fig. 4. Electrical data of PZT: (a) temperature dependence of dc-conductivity, (b)fitted-frequency dependence of ac-conductivity at various temperatures, (c) temperature dependence of ac-conductivity at various frequencies, (d) J-E at various temperatures.

Table 1
AC conductivity fitting of PZT at different temperatures.

Temperature (K)	σ_{DC} (S/m)	A	n	R^2
548	0.02	1.86×10^{-8}	0.88	0.996
573	0.029	5×10^{-8}	0.83	0.997
653	0.081	4.8×10^{-11}	0.81	0.98

3.7. J–E characteristics

The J–E characteristics study of ferroelectric ceramics helps understand their conduction mechanism as shown in Fig. 4.d. The study shows that current density increases with temperature, indicating NTCR behavior, and rapidly increases with electric field, indicating semiconducting nature. The materials allow small leakage currents and follow Ohmic behavior in low electric fields and Child's law in high fields. The conduction mechanism in high-electric fields and high-temperature regions may be a combination of these factors.

The piezoelectric measurement for the tested PZT sample was poled at 3–5 kV for 30 min. The PZT displays d33 as 129 pC/N at room temperature.

4. Conclusions

The paper presents a cost-effective and less complex PZT-ferroelectric aqueous ink with properties suitable for inkjet printers. The ink has an average particle size of 0.0480 µm, a surface area of 20.02 m^2/g, a viscosity of 1.3 cp, and a surface tension of 35.5 mN/m at 30 ^{o}C, making it suitable for fabricating electronic circuits. The electrical properties, such as electrical conductivity, dielectric constant, and modulus of the solid substance (dry ink) as a function of temperature and/or frequency, were examined. The frequency dependence of dielectric constants at various temperatures shows typical relaxor ferroelectric properties and sensitive dependence on temperature and frequency. The study reveals that the materials studied have bulk grain contributions decreasing with temperature and non-Debye-type conductivity relaxation. The AC conductivity spectrum of PZT electro ceramics follows Jonscher's universal power law, suggesting space charge accumulation and a hopping mechanism for electrical transport. The J–E curves confirm non-Ohmic and space-charge limited conduction in the material, with the nonlinear conduction mechanism. This suggests that the materials exhibit frequency-invariant-dependent electrical properties. The ceramic sample has a piezoelectric constant of d33 at ambient temperature = 149 pC/N. As a result, the dry ink's output is appropriate for producing nonlinear, high-dielectric ferroelectric ceramics for fabricating electronic circuits.

Uncited reference

[31]

CRediT authorship contribution statement

Mohamed Mustafa Dabour: Writing – review & editing, Writing – original draft, Methodology. **Khaled Faisal Qasim:** Writing – review & editing, Visualization, Supervision, Investigation, Data curation. **Mahmoud Ahmed Mousa:** Writing – review & editing, Writing – original draft, Supervision, Project administration, Conceptualization.

Declaration of Competing Interest

The authors declare no competing interests.

Data Availability

Data will be made available on request.

References

[1] L. Sanchez-Duenas, et al., A review on sustainable inks for printed electronics: materials for conductive, dielectric and piezoelectric sustainable inks, Mater. (Basel) vol. 16 (11) (2023), https://doi.org/10.3390/ma16113940.

[2] S. Gonçalves, et al., Environmentally friendly printable piezoelectric inks and their application in the development of all-printed touch screens, ACS Appl. Electron. Mater. vol. 1 (8) (2019) 1678–1687, https://doi.org/10.1021/acsaelm.9b00363.

[3] W. Wu, Inorganic nanomaterials for printed electronics: a review, Nanoscale vol. 9 (22) (2017) 7342–7372, https://doi.org/10.1039/c7nr01604b.

[4] J. Wiklund, et al., A review on printed electronics: fabrication methods, inks, substrates, applications and environmental impacts, J. Manuf. Mater. Process. vol. 5 (3) (2021), https://doi.org/10.3390/jmmp5030089.

[5] K.F. Qasim, W.A. Bayoumy, M.A. Mousa, Electrical and electrochemical studies of core–shell structured nanorods of LiMn2O4@PANI composite, J. Mater. Sci. Mater. Electron. vol. 31 (2020) 19526–19540, https://doi.org/10.1007/s10854-020-04482-5.

[6] S. Khan, L. Lorenzelli, R.S. Dahiya, Technologies for printing sensors and electronics over large flexible substrates: a review, IEEE Sens. J. vol. 15 (6) (2015) 3164–3185, https://doi.org/10.1109/JSEN.2014.2375203.

[7] B. Tiwari, T. Babu, R.N.P. Choudhary, Proceedings Piezoelectric lead zirconate titanate as an energy material: a review study, Mater. Today Proc. vol. 43 (2021) 407–412, https://doi.org/10.1016/j.matpr.2020.11.692.

[8] A.U. Naik, P. Mallick, M.K. Sahu, L. Biswal, S.K. Satpathy, B. Behera, "Investigation on Temperature-Dependent Electrical Transport Behavior of Cobalt Ferrite (CoFe2O4) for Thermistor Applications,", J. Solid State Sci. Technol. vol. 12 (2023) 053007.

[9] Z. Xiao, et al., Materials development and potential applications of transparent ceramics: A review, Mater. Sci. Eng. R. vol. 139 (May 2019) (2020) 100518, https://doi.org/10.1016/j.mser.2019.100518.

[10] P. Kour, S.K. Pradhan, P. Kumar, S.K. Sinha, M. Kar, Study of Ferroelectric and Piezoelectric Properties on Ca Doped PZT Ceramics, Mater. Today Proc. vol. 4 (4) (2017) 5727–5733, https://doi.org/10.1016/j.matpr.2017.06.037.

[11] A.J. Bell, Ferroelectrics: The role of ceramic science and engineering,", J. Eur. Ceram. Soc. vol. 28 (2008) 1307–1317, https://doi.org/10.1016/j.jeurceramsoc.2007.12.014.

[12] W. Dong, X. Lu, Y. Cui, J. Wang, M. Liu, Fabrication and characterization of microcantilever integrated with PZT thin film sensor and actuator, Thin Solid Films vol. 515 (2007) 8544–8548, https://doi.org/10.1016/j.tsf.2007.03.138.

[13] G.H. Haertling, Ferroelectric ceramics: history and technology, J. Am. Ceram. Soc. vol. 82 (1999) 797–818.

[14] X. Zhu, J. Zhu, S. Zhou, Z. Liu, N. Ming, Ferroelectric domain structures and their morphology evolution in Pb(Ni1/3Nb2/3)O3–PbZrO3–PbTiO3 piezoelectric ceramics modified by bismuth and zinc substitutions, J. Am. Ceram. Soc. vol. 91 (2008) 227–234, https://doi.org/10.1111/j.1551-2916.2007.02003.x.

[15] X. Jiang, et al., Enhanced energy storage and fast discharge properties of BaTiO3 based ceramics modified by i(Mg1/2Zr1/2)O3, J. Eur. Ceram. Soc. vol. 39 (2019) 1103–1109, https://doi.org/10.1016/j.jeurceramsoc.2018.11.025.

[16] L. Zhang, X. Hao, Dielectric properties and energy-storage performances by screen printing technique, J. Alloy. Compd. vol. 586 (2014) 674–678, https://doi.org/10.1016/j.jallcom.2013.10.107.

[17] L. Yang, X. Kong, Z. Cheng, S. Zhang, Ultra-high energy storage performance with mitigated polarization saturation in lead-free, J. Mater. Chem. A vol. 7 (2019) 8573–8580, https://doi.org/10.1039/c9ta01165j.

[18] L. Zhao, J. Gao, Q. Liu, S. Zhang, J. Li, Silver niobate lead-free antiferroelectric ceramics: enhancing energy storage density by B - site doping, ACS Appl. Mater. Interfaces vol. 10 (2018) 819–826, https://doi.org/10.1021/acsami.7b17382.

[19] L. Zhao, Q. Liu, J. Gao, S. Zhang, J. Li, Lead-free antiferroelectric silver niobate tantalate with high energy storage performance, Adv. Mater. coomunications vol. 29 (2017) 1701824, https://doi.org/10.1002/adma.201701824.

[20] H. Qi, et al., "Ultrahigh Energy-Storage Density in NaNbO3 -Based Lead-Free Relaxor Antiferroelectric Ceramics with Nanoscale Domains, Adv. Funct. Mater. vol. 1903877 (2019) 11–17, https://doi.org/10.1002/adfm.201903877.

[21] A. Tian, R. Zuo, H. Qi, M. Shi, Large energy-storage density in transition-metal oxide modified NaNbO3–Bi(Mg0.5Ti0.5)O3 lead-free ceramics through regulating the antiferroelectric phase structure, J. Mater. Chem. A vol. 8 (2020) 8352–8359, https://doi.org/10.1039/d0ta02285c.

[22] N. Kumar, A. Shukla, N. Kumar, S. Sahoo, S. Hajra, Structural, Electrical and Ferroelectric Characteristics of Bi(Fe0.9La 0.1)O3, Ceram. Int. vol. 44 (2018) 21330–21337, https://doi.org/10.1016/j.ceramint.2018.08.185.

[23] A. Xie, H. Qi, R. Zuo, A. Tian, J. Chena, S. Zhang, An environmentally-benign NaNbO3 based perovskite antiferroelectric alternative to traditional lead-based counterparts, J. Mater. Chem. C. vol. 7 (2019) 15153–15161, https://doi.org/10.1039/c9tc05672f.

[24] I.R. Abothu, S.-F. Liu, S. Komarneni, Q.H. Li, "Processing of Pb(Zr0.52Ti0.48)O3 (PZT) ceramics from microwave and conventional hydrothermal powders,", Mater. Res. Bull. vol. 34 (9) (1999) 1411–1419.

[25] B.L. Newalkar, S. Komarneni, H. Katsuki, Microwave-hydrothermal synthesis and characterization of barium titanate powders, Mater. Res. Bull. vol. 36 (2001) 2347–2355.

[26] S. Qiu, H. Fan, X. Zheng, Pb (Zr0.95Ti0.05)O3 powders synthesized by Pechini method: Effect of molecular weight of polyester on the phase and morphology, J. Sol. -Gel Sci. Technol. vol. 42 (2007) 21–26, https://doi.org/10.1007/s10971-006-1509-3.

[27] A.A. Jr, S.M. Zanetti, M.A.S. Oliveira, G.P. Thim, Effect of urea on lead zirconate titanate—Pb(Zr0.52Ti0.48)O3—nanopowders synthesized by the Pechini method, J. Eur. Ceram. Soc. vol. 25 (2005) 743–748, https://doi.org/10.1016/j.jeurceramsoc.2004.02.021.

[28] C.A. Oliveira, E. Longo, J.A. Varela, M.A. Zaghete, Synthesis and characterization of lead zirconate titanate (PZT) obtained by two chemical methods, Ceram. Int., Vol. 40, no. 1 PART B (2014) 1717–1722, https://doi.org/10.1016/j.ceramint.2013.07.068.

[29] A.L. Patterson, X-ray diffraction procedures for polycrystalline and amorphous materials, J. Am. Chem. Soc. vol. 77 (7) (1955) 2030–2031, https://doi.org/10.1021/ja01612a110.

[30] K. Faisal, S. Abdelhamed, A. Elaraby, M. Ahmed, Polyaniline impact on graphitic C3N4' s structural and physicochemical properties for high stability energy storage systems: Practical and theoretical studies, J. Ind. Eng. Chem (2024), https://doi.org/10.1016/j.jiec.2024.05.011.

[31] Abdulsamee Fawzi Abdul Aziz AL-Bayati, Study structural, dielectric and ferroelectric properties of Pb (Zr1-x Tix)O3 ceramics near the morphotropic phase boundary, Tikrit J. Pure Sci. vol. 21 (3) (Feb. 2023) 125–134, https://doi.org/10.25130/tjps.v21i3.1005.

[32] A. Khorsand Zak, W.H. Abd. Majid, Characterization and X-ray peak broadening analysis in PZT nanoparticles prepared by modified sol-gel method, Ceram. Int. vol. 36 (6) (2010) 1905–1910, https://doi.org/10.1016/j.ceramint.2010.03.022.

[33] K.F. Qasim, M.A. Mousa, Effect of oxidizer on PANI for producing BaTiO3@PANI perovskite composites and their electrical and electrochemical properties, J. Inorg. Organomet. Polym. Mater., no. 0123456789 (2022), https://doi.org/10.1007/s10904-022-02335-8.

[34] P.S. Das, P.K. Chakraborty, B. Behera, R.N.P. Choudhary, Electrical properties of Li2BiV5O15 ceramics, Phys. B Condens. Matter vol. 395 (1–2) (May 2007) 98–103, https://doi.org/10.1016/j.physb.2007.02.065.

[35] K. Parida, S.K. Dehury, R.N.P. Choudhary, Structural, electrical and magneto-electric characteristics of complex multiferroic perovskite Bi0.5Pb0.5Fe0.5Ce0.5O3, J. Mater. Sci. Mater. Electron. vol. 27 (11) (Nov. 2016) 11211–11219, https://doi.org/10.1007/s10854-016-5241-7.

[36] B.N. Parida, D. Piyush R, R. Padhee, R.N.P. Choudhary, A new ferroelectric oxide Li2Pb2Pr2W2Ti4Nb4O30: Synthesis and characterization, J. Phys. Chem. Solids vol. 73 (6) (Jun. 2012) 713–719, https://doi.org/10.1016/j.jpcs.2012.01.013.

[37] J.C. Anderson, "Dielectrics," Champan Hall Ltd, 1964.

[38] S. Nath, S.K. Barik, R.N.P. Choudhary, Electrical and ferroelectric characteristics of (LaLi)1/2(Fe2/3Mo1/3)O3, J. Mater. Sci. Mater. Electron. vol. 27 (8) (Aug. 2016) 8717–8724, https://doi.org/10.1007/s10854-016-4894-6.

[39] S. Adel, B. Cherifa, D.D. Elhak, B. Mounira, Effect of Cr 2 O 3 and Fe 2 O 3 doping on the thermal activation of un-polarized PZT charge carriers, BoletíN. la Soc. Española Cerámica Y. Vidr. vol. 57 (3) (May 2018) 124–131, https://doi.org/10.1016/j.bsecv.2017.11.001.

[40] D. Bochenek, P. Niemiec, Microstructure and physical properties of the multicomponent PZT-type ceramics doped by calcium, sodium, bismuth and cadmium, Appl. Phys. A vol. 124 (11) (Nov. 2018) 775, https://doi.org/10.1007/s00339-018-2203-3.

[41] S.C. Panigrahi, P.R. Das, B.N. Parida, R. Padhee, R.N.P. Choudhary, Dielectric and electrical properties of gadolinium-modified lead-zirconate-titanate system, J. Alloy. Compd. vol. 604 (Aug. 2014) 73–82, https://doi.org/10.1016/j.jallcom.2014.03.078.

[42] C.K. Suman, K. Prasad, R.N.P. Choudhary, Complex impedance studies on tungsten-bronze electroceramic: Pb2Bi3LaTi5O18, J. Mater. Sci. vol. 41 (2) (Jan. 2006) 369–375, https://doi.org/10.1007/s10853-005-2620-5.

[43] N. Panda, S. Pattanayak, R.N.P. Choudhary, A. Kumar, Retraction Note: Effect of La-substitution on structural, dielectric and electrical properties of (Bi0.5Pb0.5)(Fe0.5Zr0.25Ti0.25)O3, Appl. Phys. A vol. 129 (2) (Feb. 2023) 97, https://doi.org/10.1007/s00339-023-06384-9.

[44] M. Khairy, W.A. Bayoumy, K. Faisal, E.E. Elshereafy, M.A. Mousa, Electrical and Electrochemical Behavior of Binary Li4Ti5O12–Polyaniline Composite, J. Inorg. Organomet. Polym. Mater. vol. 30 (8) (2020) 3158–3169, https://doi.org/10.1007/s10904-020-01478-w.

[45] B. Behera, P. Nayak, R.N.P. Choudhary, Impedance spectroscopy study of NaBa2V5O15 ceramic, J. Alloy. Compd. vol. 436 (1–2) (Jun. 2007) 226–232, https://doi.org/10.1016/j.jallcom.2006.07.028.

[46] B. Behera, P. Nayak, R.N.P. Choudhary, Study of complex impedance spectroscopic properties of LiBa2Nb5O15 ceramics, Mater. Chem. Phys. vol. 106 (2–3) (Dec. 2007) 193–197, https://doi.org/10.1016/j.matchemphys.2007.05.036.

[47] M.A. Ali, M.M. Uddin, M.N.I. Khan, F.-U.-Z. Chowdhury, S.M. Haque, Structural, morphological and electrical properties of Sn-substituted Ni-Zn ferrites synthesized by double sintering technique, J. Magn. Magn. Mater. vol. 424 (2016) 148–154, https://doi.org/10.1016/j.jmmm.2016.10.027.

[48] D.K. Pradhan, R.N.P. Choudhary, B.K. Samantaray, Studies of structural, thermal and electrical behavior of polymer nanocomposite electrolytes, Express Polym. Lett. vol. 2 (9) (2008) 630–638, https://doi.org/10.3144/expresspolymlett.2008.76.

[49] S. Aziz, O. Abdullah, S. Hussein, H. Ahmed, Effect of PVA blending on structural and ion transport properties of CS:AgNt-based polymer electrolyte membrane, Polym. (Basel) vol. 9 (11) (Nov. 2017) 622, https://doi.org/10.3390/polym9110622.

[50] P. Goel, K.L. Yadav, A.R. James, Double doping effect on the structural and dielectric properties of PZT ceramics, J. Phys. D. Appl. Phys. vol. 37 (2004) 3174–3179, https://doi.org/10.1088/0022-3727/37/22/019.

[51] J. Isasi, M.L. Lopez, M.L. Veiga, E. Ruiz-Hitzky, C. Pico, Structural,

characterization and electrical properties of a novel defect pychlore, J. Solid State Chem. vol. 116 (1995) 290–295.
[52] N. Kumar, A. Shukla, N. Kumar, R.N.P. Choudhary, Structural, electrical and magnetic properties of eco-friendly complex multiferroic material: Bi (Co0.35Ti0.35Fe0.30)O3, Ceram. Int. vol. 45 (1) (2019) 822–831, https://doi.org/10.1016/j.ceramint.2018.09.249.
[53] J. ROSSMACDONALD, Note on the parameterization of the constant-phase admittance element, Solid State Ion. vol. 13 (2) (May 1984) 147–149, https://doi.org/10.1016/0167-2738(84)90049-3.
[54] S. Joshi, A. Shukla, N. Kumar, R.N.P. Choudhary, Nd substitution response on structural, dielectric, and electrical features of bismuth iron titanate, Ceram. Int. vol. 50 (1) (2024) 1643–1654, https://doi.org/10.1016/j.ceramint.2023.10.259.
[55] A.R. James, J. Subrahmanyam, K.L. Yadav, Structural and electrical properties of nanocrystalline PLZT ceramics synthesized via mechanochemical,“ *J. Appl. D Appl. Phys.* vol. 39 (2006) 2259–2263, https://doi.org/10.1088/0022-3727/39/10/039.
[56] N. Kumar, A. Shukla, N. Kumar, S. Sahoo, S. Hajra, R.N.P. Choudhary, Structural, electrical and ferroelectric characteristics of Bi(Fe0.9La 0.1)O3, Ceram. Int. vol. 44 (17) (2018) 21330–21337, https://doi.org/10.1016/j.ceramint.2018.08.185.
[57] N. Kumar, A. Shukla, R.N.P. Choudhary, Structural, dielectric, electrical and magnetic characteristics of lead-free multiferroic: Bi(Cd0.5Ti0.5)O3–BiFeO3 solid solution,", J. Alloy. Compd. vol. 747 (2018) 895–904, https://doi.org/10.1016/j.jallcom.2018.03.114.
[58] P. Chaitanya, A. Shukla, L. Pandey, Determination of equivalent circuit model components of piezoelectric materials by using impedance spectroscopy, Integr. Ferroelectr. vol. 150 (1) (2014) 88–95, https://doi.org/10.1080/10584587.2014.874274.
[59] E. Kabir, M. Khatun, R.J. Mustafa, K. Singh, M. Rahman, AC electrical conductivity and dielectric properties of doping induced molecular ferroelectric diisopropylammonium bromide AC electrical conductivity and dielectric properties of doping induced molecular ferroelectric diisopropylammonium bromide, Mater. Res. Express vol. 6 (2019) 096306.
[60] K.F. Qasim, M.A. Mousa, Electrical and dielectric properties of self-assembled polyaniline on barium sulphate surface, Egypt. J. Pet. vol. 30 (2021) 9–19, https://doi.org/10.1016/j.ejpe.2021.09.001.
[61] K.F. Qasim, M.A. Mousa, Physicochemical Properties of Oriented Crystalline Assembled Polyaniline/Metal Doped Li4Ti5O12 Composites for Li-ion Storage, J. Inorg. Organomet. Polym. Mater. vol. 33 (9) (2023) 2601–2617, https://doi.org/10.1007/s10904-023-02720-x.
[62] R. Padhee, P.R. Das, B.N. Parida, R.N.P. Choudhary, "Structural, Dielectric and Pyroelectric Properties of Praseodymium Based Complex Tungsten Bronze Ferroelectrics, Ferroelectrics vol. 437 (2012) 160–170, https://doi.org/10.1080/00150193.2012.738588.
[63] P. Chaitanya, O.P. Thakur, V. Kumar, A. Shukla, L. Pandey, Equivalent circuit model of a PbZr0.6Ti0.4O3 ceramic using impedance spectroscopy, J. Ceram. Process. Res. vol. 12 (3) (2011) 247–258.
[64] A.E.S. Etman, A.M. Ibrahim, F.A.Z.M. Darwish, K.F. Qasim, A 10 years-developmental study on conducting polymers composites for supercapacitors electrodes: A review for extensive data interpretation, J. Ind. Eng. Chem. vol. 122 (2023) 27–45, https://doi.org/10.1016/j.jiec.2023.03.008.
[65] S. Dagar, A. Hooda, S. Khasa, M. Malik, Structural refinement, investigation of dielectric and magnetic properties of NBT doped BaFe12O19 novel composite system, J. Alloy. Compd. vol. 826 (Jun. 2020) 154214, https://doi.org/10.1016/j.jallcom.2020.154214.
[66] B.K. Barick, K.K. Mishra, A.K. Arora, R.N.P. Choudhary, D.K. Pradhan, Impedance and Raman spectroscopic studies of (Na0.5Bi0.5)TiO3, J. Phys. D. Appl. Phys. vol. 44 (35) (Sep. 2011) 355402, https://doi.org/10.1088/0022-3727/44/35/355402.
[67] P. Mallick, S.K. Satpathy, B. Behera, Study of structural, dielectric, electrical, and magnetic properties of samarium-doped double perovskite material for thermistor applications, Braz. J. Phys. vol. 52 (6) (2022), https://doi.org/10.1007/s13538-022-01190-9.
[68] K. Liu, H. Wang, Y. Wu, Y. Wang, C. Yuan, Preparation and properties of gamma-PVDF/lead zirconium titanate composites, Polym. (Guildf.) vol. 281 (April) (2023) 126091, https://doi.org/10.1016/j.polymer.2023.126091.
[69] M. Prabu, A. Chandrabose, Complex impedance spectroscopy studies of PLZT (5/52/48) ceramics synthesized by sol–gel route, J. Mater. Sci. Mater. Electron. vol. 24 (11) (Nov. 2013) 4560–4565, https://doi.org/10.1007/s10854-013-1442-5.
[70] B. Pati, R.N.P. Choudhary, P.R. Das, Phase transition and electrical properties of strontium orthovanadate, J. Alloy. Compd. vol. 579 (2013) 218–226, https://doi.org/10.1016/j.jallcom.2013.06.050.
[71] P. Mallick, S.K. Biswal, S.K. Satpathy, B. Behera, Structural, electrical and thermistor behavior of BiFeO3–PbZrO3 for energy-storage devices, Emerg. Mater. Res. vol. 12 (2023) 3–11, https://doi.org/10.1002/0471684228.egp10814.